An integrated QCM-based narcotics sensing microsystem†

Thomas Frisk,[a] Niklas Sandström,[a] Lars Eng,[b] Wouter van der Wijngaart,[a] Per Månsson[b] and Göran Stemme[a]

Received 10th January 2008, Accepted 3rd June 2008
First published as an Advance Article on the web 13th August 2008
DOI: 10.1039/b800487k

We present the design, fabrication and successful testing of a $14 \times 14 \times 4$ mm^3 integrated electronic narcotics sensing system which consists of only four parts. The microsystem absorbs airborne narcotics molecules and performs a liquid assay using an integrated quartz crystal microbalance (QCM). A vertically conductive double-sided adhesive foil (VCAF) was used and studied as a novel material for LOC and MEMS applications and provides easy assembly, electrical contacting and liquid containment. The system was tested for measuring cocaine and ecstasy, with successful detection of amounts as small as 100 ng and 200 ng, respectively. These levels are of interest in security activities in customs, prisons and by the police.

Introduction

Detection and monitoring of hazardous airborne molecules have become an important part in public health care, military and customs activities, security surveillance in public buildings and transportation, and in environmental monitoring.

Police, customs personnel, security personnel and other authorities need detection equipment in order to detect the presence of theses hazardous substances in public areas.

Important requirements from the applications mentioned above include:

- Molecules of interest are *e.g.* narcotics, explosives, pollutants, allergens, and pathogens.
- Portability of the instrument needed in field work or for use in ubiquitous sensor networks, reducing the need for dedicated machine area and external power supply.
- Rapid response from the instrument is important as passengers or citizens should not be unnecessarily delayed.
- Simplicity in operation of the instrument.
- Robustness to normal handling procedures and harsh environments.
- Reliable detection.

Airborne compounds can be detected with miniaturized electronic sensors, and the majority of the demands and features listed above can be met with microfluidic analysis systems.

Previous microsystems for air monitoring include three absorption schemes.

Firstly, usage of an open liquid reservoir with passive particle absorption has been suggested by both Michalzik *et al.*[1] and Kößlinger *et al.*[2] Secondly, passively controlled surface tension based microfluidic interfaces for airborne sample-to-liquid absorption have been demonstrated by ourselves[3] and by Sridharamurthy *et al.*[4] In these works, surface tension provides robustness to the device so that it will withstand pressure variations during manual handling. Finally, systems with active liquid manipulation can be utilized to capture and transfer airborne particles to microfluidic systems. Desai *et al.*[5] demonstrated airborne particle sampling with a liquid meniscus interface with DEP driven particle capture through the air–liquid interface. Recently, Zhao *et al.*[6] showed particle trapping with EWOD droplet sweeping.

The above capturing methods each have their advantages and disadvantages.

With open liquid reservoirs, the interfacial area is large but sensitive to external influence since the liquid–air surface is easily disturbed. Such systems cannot offer robustness in terms of pressure variation tolerance or invariance to gravitation changes (*i.e.* abrupt movement of the device). Surface tension based passive systems offer a stable air–liquid interface for absorption of airborne particles and substances. However, in the work by Frisk *et al.*[3] transport of the analytes in the fluidic system to the downstream sensor array reduces the possibility for a rapid response signal. Sridharamurthy *et al.*[4] are somewhat limited in the size of their exposed area.

Active liquid manipulation, as shown in the works of Desai[5] and Zhao,[6,7] utilize a moving liquid front, requiring electrical manipulation of particles, the liquid or its constituents, with absorption taking place when the liquid reaches particles on the surface. By actively controlling the air–liquid interface, stability problems are less compared to using open reservoirs but the complexity of such devices negatively affects the potential for portability.

The quartz crystal microbalance (QCM)[2,8–16] is a commonly used biosensor and is commercially used for detector applications.[17] Moreover, it is a well-known, low-cost and well established microsensor principle.[18–20]

Problems encountered in commercial sensors systems are long transport paths through tubing, valves, *etc*, resulting in reagent depletion through parasitic binding and in sample dispersion. Furthermore, difficulties in integration of many

[a]*Microsystem Technology Lab, KTH - Royal Institute of Technology, Stockholm, Sweden*
[b]*Biosensor Applications AB, Solna, Sweden*

† Electronic supplementary information (ESI) available: VCAF as a MEMS material. See DOI: 10.1039/b800487k

stand-alone components hinder development of portable instruments.

Our proposed solution includes a passively controlled air–liquid adsorption interface for molecules of interest in direct conjunction with a highly sensitive QCM. The miniaturised liquid environment trapped between the interface and the sensor enables an immunohistological assay, which can be made highly selective.

Sensor design and measurement principle

The sensor system presented herein consists of a quartz crystal mounted to a silicon chip and covered by a protective polymer cap by using double-sided vertically conductive adhesive foil (VCAF), see Fig. 1. The silicon chip serves several functions: it gives rigid support to all device parts, it accommodates microchannels for transport of buffer liquid and electrical paths to the crystal electrodes through the VCAF, and it defines a robust air–liquid interface where airborne molecules can become absorbed into the liquid. The quartz crystal is a shear mode electromechanical oscillator, with the resonance frequency dependent on the mass of the material attached to its surface. Piezoelectric excitation is provided through the top and bottom electrodes with wrap-around contact pads. The VCAF adhesively bonds both the quartz crystal and the protective polymer cap to the silicon chip and seals the liquid paths. The anisotropically conductive property of the foil provides electrical connection between the silicon chip and the QCM, and electrical isolation to the rest of the system, which allows for easy external contacting to the device. Further information about the foil used herein can be found in the electronic supplementary information.† The polymer cap gives protection to the QCM from external influences without making any mechanical contact to it. Through the cap, electric and fluidic connections are made and direct exposure of the sensing parts of the device is avoided.

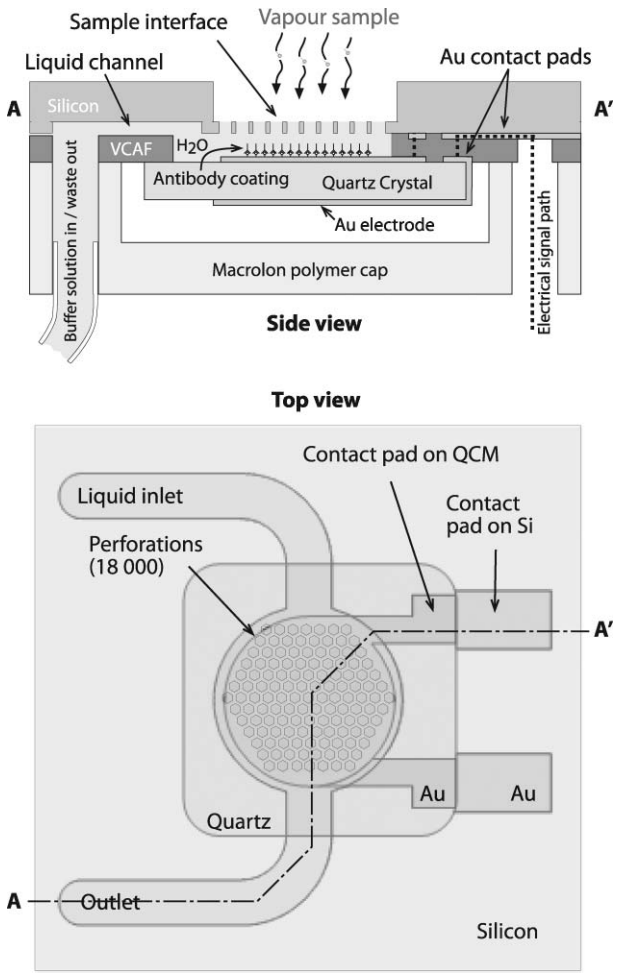

Fig. 1 Schematic cross-sectional (top) and top view (down) of the electronic sensor system. It consists of a perforated silicon chip, microchannels and contact pads. A QCM is mounted to the silicon with a vertically conductive adhesive foil. The cavity between the silicon and the crystal is filled with buffer liquid. The diaphragm perforations at the air–liquid sample interface form Laplace valves, keeping the liquid meniscus stable to avoid flooding or bubble introduction. The backside of the crystal is protected with a polymer cap, accommodating tubing and wiring.

The sensor is based on a QCM with a competitive immunoassay developed by Biosensor Applications AB, Stockholm, Sweden. The assay consists of drug molecules, antibodies (Ab), and surface immobilized antigens (Ag). The antibodies have a higher affinity to the drug molecules than to the antigens and consequently more Ab–drug than Ab–Ag complexes are formed in the presence of all three types of molecules. This assay is used to enhance the signal read-out, *i.e.* change in mass at the sensor surface, upon detection of drug molecules since the antibodies have a larger mass than the drug molecules.

The working principle of the device, from surface immunoactivation to a detection read-out, is illustrated in Fig. 2 and marked with numbers in the following text. Prior to the drug measurement, the QCM-surface is pre-coated with antigens (1). Then, antibodies are introduced *via* liquid droplets on the air–liquid interface, where they are absorbed into the liquid and diffuse to the QCM. When they reach the QCM-surface they bind to the antigens and form immobilized complexes (2). This causes an increased surface-mass of the sensor which can be detected as a decrease of the QCM resonance frequency. In a commercial application, a fibreglass sheet or filter is used to collect the drug sample.[21,22] The drug collection method will not be further discussed here, but there are several methods available, including suction, sweeping *etc*. In this study, a fibreglass sheet prepared with the drug sample was used (3). During a measurement, the sample collection sheet is brought in close proximity to the liquid interface. Local heating of the sheet causes vaporization of the drug, which is transported to the air–liquid interface through convection and diffusion (4). The airborne drug molecules impact on the liquid surface and become absorbed (5). Mainly diffusive flow, but with contribution from convective and Marangoni flow, further transports the drug molecules through the buffer liquid to the QCM surface. In competition with the immobilized antigens, the drug molecules react with the antibodies (6). The formed drug–Ab complexes release from the sensor surface (7), leading to a decrease in surface-mass and consequently a measurable increase in resonance frequency of the QCM (8). With a constant buffer flow present in the device, non-bound antibodies and drug–Ab complexes are transported to the waste outlet after antibody loading and after drug–Ab reaction, respectively.

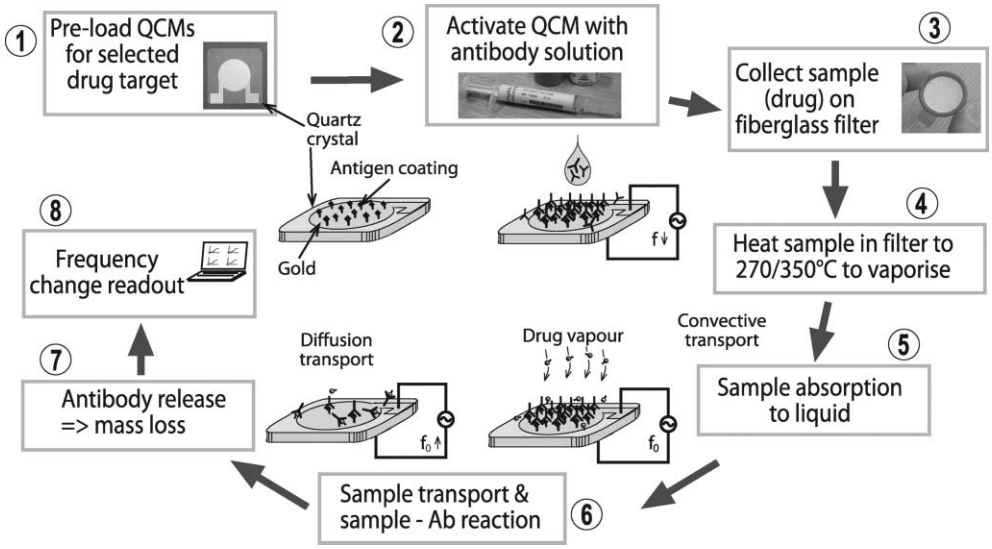

Fig. 2 The working principle for drug sample detection with QCM-based mass-loss detection. Note that the immunoassay is done in liquid phase and only on one side of the quartz crystal. Rinsing is done through a continuous liquid flow over the QCM surface, which will also compensate for evaporation during heating of sample filter. Resonator frequency changes correspond to changes in surface bound mass.

Theory and design considerations

Definitions and parameters

In this section, a few essential aspects of the device are discussed and translated into design considerations. Mechanical aspects relate to the mechanical robustness, which is defined by the materials used and the geometric design. A mechanically important part is the perforated silicon diaphragm. A critical condition that appears under liquid pressure load is the deflection, w, of the diaphragm. This can occur during priming or sudden drying of the interface when exposed to a heat pulse. The amount of centre deflection, w_0, under a certain pressure load is influenced by the diaphragm thickness, h, and its radius, a, and by the material properties given by the Young's modulus, E, and the Poisson's ratio, ν, as follows:[23]

$$w_0 \propto \frac{a^2(1-\nu)}{Eh^3} \quad (1)$$

The diaphragm thickness and radius should be chosen such that the centre deflection is less than the spacing, t, between the diaphragm and the underlying crystal, in our case defined by the thickness of the VCAF. Moreover, although their influence cannot be readily expressed analytically in eqn (1), the diameter, d, and the pitch, b, of the perforations strongly influence the mechanical stiffness of the diaphragm and they must be taken into consideration. Thus, from a pure mechanical viewpoint, the diaphragm should be stiff, thick, and have a suitable density of the perforations to withstand deformations caused by pressure variations originating from the liquid flow and the capillary forces. Silicon, with its high Young's modulus of approximately 130 GPa[24] and excellent microfabrication potential, was chosen as the material for the diaphragm of this device.

The diaphragm thickness and the perforation size and pitch also affect the total wet diaphragm surface area, A_{wet}, around the sensor site which may act as a parasitic binding area for the drug molecules, thus reducing the available amount of reacting molecules in the immunoassay. In our design, A_{wet} constitutes 66% of the total wet areas of the assay chamber. The perforation size and pitch also affects the total dry diaphragm surface area, A_{dry}, which may act as a parasitic binding area for airborne molecules. The fill factor in this design is 45.6% wet area and 54.4% dry area seen by the airborne molecules.

After absorption of drug molecules at the air–liquid interface, the molecules must move through the perforations and the layer of liquid to reach the sensor surface. In this study, only transport by diffusion is considered although heat convective transport and Marangoni flow may contribute. The total diffusion length, L, *i.e.* the distance from the air–liquid interface to the surface of the QCM, is critical since it greatly affects the transport time of diffusion. In this case, the diffusion length is the sum of t and h, and thus these parameters must be chosen to be as low as possible to allow for fast transport of the drug molecules to the sensor surface and thereby enable a rapid analysis of the sample contents. The average diffusion transport time, τ, through the liquid can be estimated by the Einstein–Smoluchowski equation for three dimensional Brownian motion along one axis:

$$\tau = \frac{L^2}{2D} \quad (2)$$

Here, D is the diffusion constant. In our design, τ was calculated to be approximately 2.7 and 3.6 s for cocaine and ecstasy molecules, respectively ($D_{cocaine} = 9.1 \times 10^{-10}$ m^2 s^{-1}, $D_{ecstasy} = 6.9 \times 10^{-10}$ m^2 s^{-1}, $L = t + h = 50 + 20 = 70$ μm). An illustration of the sample transport in the assay chamber is shown in Fig. 3. In conclusion, the thickness of the diaphragm and the perforation diameter and spacing should be designed to withstand pressure loads causing a centre deflection that leads to contacting with the QCM, but with the consideration to minimize the parasitic areas and the total diffusion length for the drug molecules.

The surface tension, or the surface free energy, is of key importance for the handling robustness of the device. The liquid

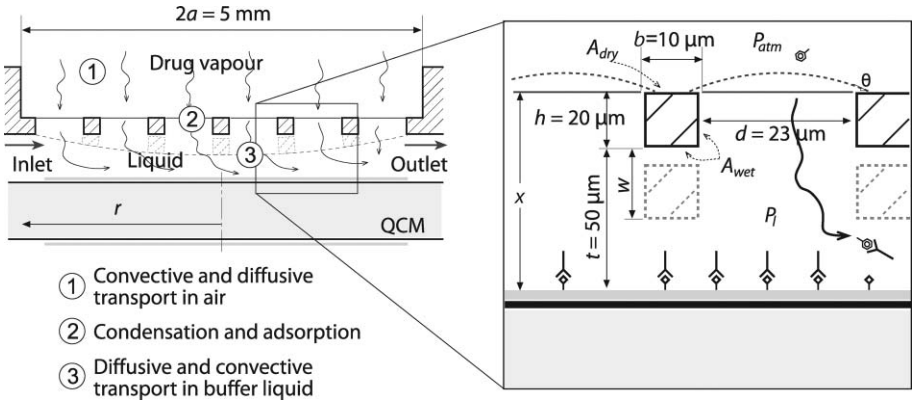

Fig. 3 A cross-cut schematic illustration of the assumed transport in the device. System model with parameters and characteristic dimensions are indicated. Note: the dotted line depicts a deflection of the diaphragm of distance w.

contact angle, θ, is given by the interfacial energies in the system according to Young's equation:

$$\gamma_{SL} + \gamma_{LG}\cos\theta - \gamma_{SG} = 0 \quad (3)$$

Here, γ_{SL} is the solid–liquid interfacial energy, γ_{LG} is the liquid–gas interfacial energy, γ_{SG} is the solid–gas interfacial energy, and θ is the wetting contact angle of the liquid. From a fluidic perspective, one would ideally like to have the wetted areas of the device hydrophilic ($\theta < 90°$) to allow for easy and rapid filling when using aqueous solutions and to avoid air bubble introduction when low liquid pressure P_l occur. However, the dry areas of the diaphragm should preferably be hydrophobic ($\theta > 90°$) to increase the Laplace burst pressure, *i.e.* robustness against flooding. The surface character of the materials in the device also affects the level of parasitic binding and consequently the loss of narcotic sample. Surface modifications and chemical treatments of the materials are possible, *e.g.* through passivation, oxidation, adding blocking agents *etc.*, to reduce those parasitic effects. However, such methods have not been evaluated for the tested device.

Surface tension provides robustness to the air–liquid interface, which is necessary for tolerating pressure and flow variations during operation that could lead to a collapse of the interface. Each perforation functions as a static Laplace valve, keeping the liquid meniscus in a fixed position. However, large negative or positive pressure loads can break the valve and subsequently cause air introduction or flooding,[3,25,26] respectively. In the case of flooding, the required positive pressure load, P_{L+}, is given by a modified Young–Laplace equation:[27,28]

$$P_{L+} = \frac{4\gamma_{LG}}{d}\sin\theta \quad (4)$$

It is seen that a smaller diameter of the perforations allows for greater pressure loads before flooding occurs.[29] Controlled flooding of the device can be actively used in a rinsing procedure of the dry areas of the diaphragm, but should not occur unintentionally.[3] Introduction of air bubbles in the liquid is more problematic because this can block the downstream fluidic system. The negative pressure load, P_{L-}, that is required for bubble introduction can be calculated as:

$$P_{L-} = -\frac{4\gamma_{LG}}{d} \quad (5)$$

In this case, the radius of the perforations is equal to the critical radius for bubble formation. According to eqn (4) and (5), the required pressure loads to cause flooding or bubble introduction in the design are 6.3 kPa and −12.7 kPa, respectively (for $\theta = 30°$ and $\gamma = 0.073$ N m^{-2}). Thus, the device theoretically tolerates pressure fluctuations of up to approximately 5 kPa for an operational pressure of 1 kPa before malfunctioning, unless contacting to the QCM due to diaphragm deflection occurs for lower pressure loads. Note that the presence of large amounts of narcotics can cause a dramatic shift in surface tension of the buffer solution. The properties of the system, *e.g.* the contact angle, may then alter and cause unpredictable and difficult to control flooding or bubble introduction.

Dry-out of the buffer liquid can cause deterioration of the antibody coating on the QCM, but with a continuous flow of liquid the problem is avoided. Another feature of the continuous buffer flow is to flush away unbounded molecules at the sensing crystal surface. The flow rate has an upper limit as there must be sufficient time for the sample to diffuse and react with the antibodies on the QCM surface. The lower flow rate limit is set by the allowable time to reset the chemical conditions in the buffer solution, *e.g.* between two separate measurements, but also to sustain the chemical conditions during active measurements, *e.g.* to prevent changes in salinity due to evaporation. For an applied pressure of 1 kPa, the resulting flow rate at the inlet and outlet of the device is measured to 0.35 µl min^{-1}. This results in a residence time of the liquid above the active sensor area in the order of 3 min. Parameters of both mechanical and functional characteristics with impact on critical conditions, as well as resulting failure modes and typical values of the device, are summarized in Table 1.

Simulations of sample transport in liquid

To study the combined effects of diffusion and convective flow on the transport of drug molecules from the air–liquid interface to the sensing surface, a two dimensional finite element analysis (Multiphysics 3.4, Comsol AB, Stockholm, Sweden) was conducted. The main focus was to investigate the molecule flux to the sensing surface in relation to the liquid flow necessary to reset the system prior to a new measurement. Equations for convection and diffusion, incompressible Navier–Stokes, and

Table 1 The influence of parameters on typical critical conditions

	Parameters							
Critical conditions	Diaphragm radius, ***a*** (2.5 mm)	Diaphragm thickness, ***h*** (20 μm)	Diaph.-QCM spacing, ***t*** (50 μm)	Perforation diameter, ***d*** (23 μm)	Perforation pitch, ***b*** (33 μm)	Contact angle, θ (30°)	Liquid pressure[a], P_l (1 kPa)	Failure modes	Typical values[b]
Laplace pressure[a], P_L	—	—	—	$P_L \sim 1/d$	—	$P_{L+} \sim \sin\theta$	$P_{L-} \leq P_l \leq P_{L+}$	Flooding	$P_{L+} = 6.3$ kPa
								Bubble introduction	$P_{L-} = -12.7$ kPa
Diaphragm deflection, w	$w_0 \sim a^2$	$w_0 \sim 1/h^3$	$w_0 \leq t$	—	—	—	$w \sim P_l$	Membrane rupture	—
								Diaph.-QCM contact	
Diffusion time, τ	—	$\tau \sim (h + t)^2$	$\tau \sim (h + t)^2$	—	—	—	—	Low transport efficiency	$\tau = 2.7$–3.6 s
Dry parasitic area, A_{dry}	$A_{dry} \sim a^2$	—	—	$A_{dry} \sim d^2$	$A_{dry} \sim b^2$	—	—	Sample lost prior to adsorption	$A_{dry} = 54\%$ of dry area
Wet parasitic area, A_{wet}	$A_{wet} \sim a^2$	$A_{wet} \sim h$	$A_{wet} \sim t$	$A_{wet} \sim d^2$	$A_{wet} \sim b^2$	—	—	Sample lost prior to reaction	$A_{wet} = 66\%$ of wet area

Note: The parameter values indicated within brackets are based on the characteristics of the fabricated device. [a] Pressures are indicated relative to atmospheric conditions. [b] Values estimated based on calculations from the characteristics of the fabricated device.

partial differential equations (PDE) for weak form boundaries were coupled in the Multiphysics mode. The system was modelled as a perforated diaphragm containing 21 perforations that were 20 μm deep, 25 μm wide, and separated by 10 μm. Simulation showed that no entrance or edge effects were visible 10 perforations from the inlet and the system could be considered to be in the fully-developed region.[30] The diaphragm was positioned 50 μm above a coated surface with antibodies. A constant parabolic flow of water, with a defined maximum velocity u_{max}, was set at the left inlet boundary and zero pressure at the right outlet boundary of the model. On top of each perforation, which represents the air–liquid interface in the system, a constant inward flux of cocaine molecules was set for 5 s, representing the heat pulse during the experiments. The total amount of drug that was applied in the simulations corresponds to a supply of 0.19–200 ng of drug to the air–liquid interface in the real system with more than 18 000 perforations. A surface reaction between the antibodies and the drug was defined at the lower boundary of the model including the concentration of drug in the liquid, c, the initial surface concentration of antibodies, θ, the concentration of formed antibody–drug complexes at the surface, c_s, and the adsorption and desorption rate constants, k_{ads} and k_{des}, respectively. The model with boundary conditions is shown in Fig. 4.

To study the transport of drug samples, properties for cocaine and cocaine-specific IgG antibody molecules were simulated, with constants shown in Table 2. The affinity of the antibody to cocaine is much higher than to the surface bound antigen and thus it is assumed that when a cocaine molecule reaches the sensing surface, a cocaine–antibody complex is formed only according to the rate of the reaction kinetics of the antibody and the cocaine and the complex is subsequently released to the liquid. The reaction kinetics of the surface bound antigen and the antibody is considered to have minimal influence and is thereby neglected.

The simulations show that during the first 5 s, the concentration of cocaine molecules in the water increases and the maximum value is found at the air–liquid interface. The inward flux of narcotics stops at 5 s, and subsequently the drug concentration profile between the perforations and the sensor surface equalizes, see Fig. 5a and b. In a region close to the antibody-coated surface, the drug concentration maximum is reached after 6 s, see Fig. 5c. The concentration of formed and released cocaine–antibody complexes at the sensing surface increases until it reaches the same concentration as the initial surface concentration of antibodies (when the amount of applied drug is in the range of 1.5–200 ng), indicating that the surface is depleted from antibodies, see Fig. 5. The depletion occurs prior to the maximum concentration of the drug being reached above the surface. When the amount of applied sample is less than 1.5 ng the reaction is concentration dependent. In conclusion, the simulations indicate that the diffusive flux of cocaine molecules overcomes the lateral convective transport in the buffer solution and thus the resident time of the drug molecules in the real system is most likely sufficient for the molecules to be transported and react at the QCM surface. Furthermore, the system tolerates substantial losses of cocaine molecules to *e.g.* wet and dry parasitic areas and still an enough amount of molecules will most likely be able to reach the sensing

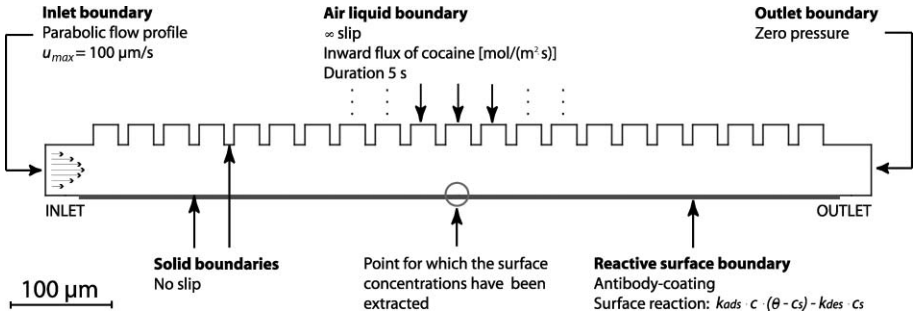

Fig. 4 Simulation model of the diaphragm containing 21 perforations located 50 µm above a reactive surface coated with antibodies. A lateral parabolic flow of water is applied between the diaphragm and the bottom surface from the left to the right hand side of the model. Drug molecules enter from the top of the perforations by an inward flux and diffuse down to the bottom surface where they interact with the antibodies. The indicated measurement point corresponds to the values presented in Fig. 5c and 5d.

Table 2 Constants for cocaine molecules and antibodies used in the FEM simulations

Constant	Value	Unit	Description
k_{ads}	1.25×10^{2}	m^3 per mol s^{-1}	Adsorption rate constant for cocaine–Ab
k_{des}	2×10^{-3}	$1\ s^{-1}$	Desorption rate constant for cocaine–Ab
θ	1.89×10^{-8}	mol m^{-2}	Initial surface concentration of Ab[a]
D	9.1×10^{-10}	$m^2\ s^{-1}$	Diffusion constant of cocaine

[a] Considered as an ideal case with a total coverage of antibodies having a hydrodynamic radius of 5.3 nm.

surface and saturate it. The overall residence time for the buffer liquid in the system of 3 min is concluded to be a sufficient time window for the complete operation: heat pulse, the air transport, the condensation and absorption of drug molecules to the liquid, the diffusive transport in the liquid, and the competitive immunoassay.

The Peclet and Dahmköler numbers[30] were estimated to $Pe = 3.8$ and $Da = 0.18$, respectively, indicating that the system will have some lateral convective transport, $Pe < 10^2$, but is mainly reaction dependent since $Da < 1$.

Materials and methods

Device fabrication

The system consists of the following four parts: the silicon chip including the diaphragm, the VCAF, the QCM, and the protective polymer cap, see Fig. 6.

The system builds on a micromachined silicon-on-insulator (SOI, 20/1.5/500 µm) substrate containing the air–liquid interface for airborne sample capturing, electrical contacts to the QCM, and fluidic channels. The substrate chip was micromachined with standard methods, including wet thermal oxidation (1 µm, 1100 °C, DI, 10 h), gold deposition (1000 Å Ti, 1000 Å Pt, 1 µm Au), lift-off, photolithography, and double-sided deep reactive ion etching.

After machining, the 10×10 mm chip contained a bulk silicon frame with two gold contact areas and two 20 µm deep fluidic channels, and a diaphragm with radius $a = 2.5$ mm and thickness $h = 20$ µm formed in the centre of the chip, see Fig. 7. The complete diaphragm was machined to contain perforations with diameter $d = 25$ µm and pitch $b = 33$ µm.

A 50 µm thick VCAF (3M 9703 Electrically Conductive Adhesive Transfer Tape, 3M, St. Paul, MN, USA) layer was punched to define access ports and interface and was taped on the substrate surface. A commercially available 8×8 mm^2 QCM (Biosensor AB, Solna, Sweden) with wrap-around gold electrodes was pre-coated with antigens (Biosensor AB, Solna, Sweden). It was manually aligned and placed on the VCAF. A pressure of 0.10 MPa was applied to the quartz crystal and the silicon to ensure proper bonding. Finally, a precision milled macrolon cap with openings for fluidic and electrical interfacing and a hollow compartment for the QCM was added to protect the backside and simplify tube connection. Tubing (Portex nylon tube, inner diameter 0.56 mm, outer diameter 1 mm) was fitted into two 1 mm in diameter liquid supply holes in the polymer cap for liquid supply of the chemical buffer and waste removal. Spring-loaded gold pins through holes in the polymer cap formed the electrical contacts to an electric oscillator read-out circuit.

Drug detection

The device was coupled in a fluidic setup with a liquid reservoir upstream, and a syringe pump downstream. A phosphate buffer saline (PBS) solution, 137 mM NaCl, 10 mM phosphate, 2.7 mM KCl, pH 7.4 was continuously hydrostatically pumped through the two fluidic ports of the device at 0.35 µl min^{-1}. 50 µl antibody solution (anti-MDMA (ecstasy) or anti-cocaine IgG, 0.1 g l^{-1} in PBS, Biosensor AB, Solna, Sweden) was applied onto the air–liquid sample interface, according to the principle shown in Fig. 2. A brief washing step with PBS followed. Fibreglass filter sheets (Biosensor AB, Solna, Sweden) containing drug traces were positioned approximately 500 µm above the interface. They were exposed to an 8 s heat pulse of 270 °C (cocaine) or 5 s at 350 °C (MDMA) to evaporate the sample from the filter. Upon interaction of the sample with the antibodies on the QCM, a

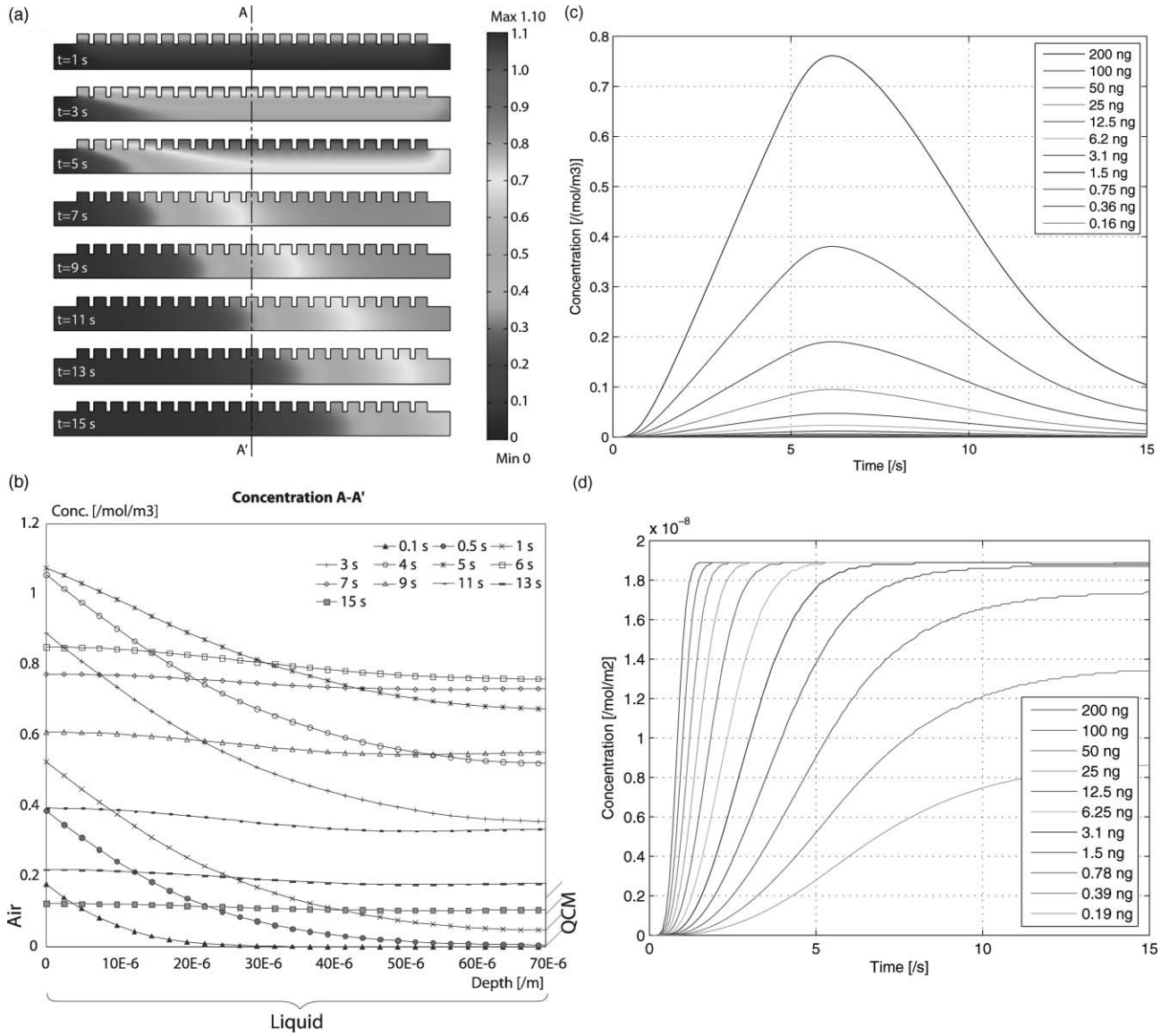

Fig. 5 (a) Plots of the concentration of cocaine molecules in the solution at 0–15 s (concentration indicated by the bar on the right-hand side [mol m^{-3}]). An inward flux of cocaine molecules is set at the air–liquid interface at 0–5 s, and subsequently the molecules are flushed away by the convective flow. The cut A–A′ indicates where the concentration is measured for the results shown in Fig. 5b. (b) Concentration of cocaine molecules in the liquid over cut A–A′. The air–liquid interface (left side) and the QCM surface (right side) are separated by 70 μm. The concentrations are plotted from 0–15 s, where a shift in the concentration profile is visible after 5 s when the inward flux of cocaine molecules at the air–liquid interface stops. (c) Concentration of cocaine molecules in the solution just above the surface of the QCM for varying applied amounts of drug during 15 s of simulation. The concentration reaches a peak at approximately 6 s, 1 s after that the inward flux of cocaine molecules stops; thereafter, the molecules are flushed away due to convective flow. Note: the point where data has been extracted for Fig. 5c and d is depicted in Fig. 4. (d) Concentration of formed cocaine–antibody complexes at the sensing surface for varying applied amounts of drug during 15 s of simulation. The surface is depleted from free antibodies at 1.5 s for 200 ng of cocaine. Depletion is achieved for all samples with a mass larger than approximately 1.5 ng of cocaine. For lower amounts of cocaine, the system becomes concentration dependent.

custom made oscillator circuit measured the baseline frequency shift (sampling rate 5 samples per second).

Results

Device robustness

Varying pressures due to flow variations or start/stop of the liquid supply when running or handling the device did not cause problems. The liquid meniscus at the air–liquid interface was kept stable by the diaphragm and the robustness of the device at hand was good. Furthermore, the mechanical strength of the diaphragm was found to be sufficient; during normal operation no diaphragm breakage or contact to the quartz crystal was observed. During filling, bubbles accidentally introduced *via* the inlet channel escaped through the diaphragm perforations. If bubbles were observed in the outlet channel, a temporary reversal of the flow resulted in a bubble escaping through the diaphragm perforations.

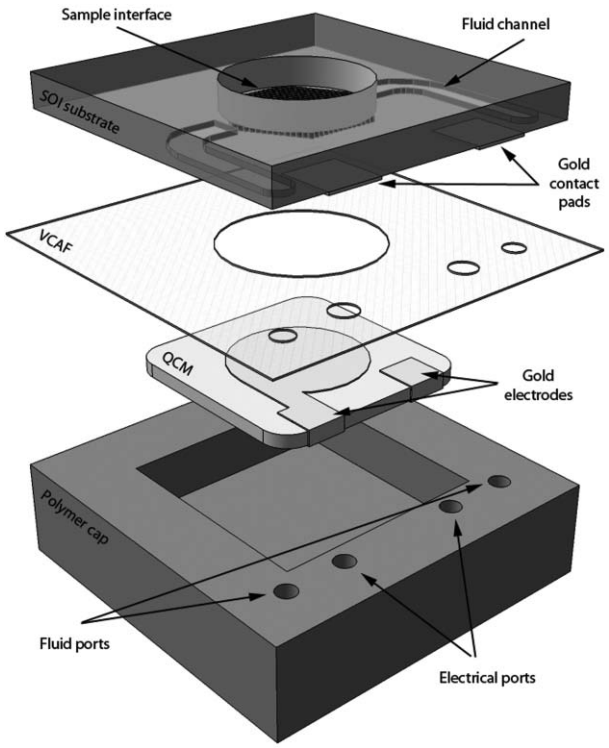

Fig. 6 Exploded to scale view of the designed four-component system: the silicon substrate with the diaphragm sustaining the air–liquid interface and the fluidic channels (10 × 10 mm and 525 µm thick), the VCAF (50 µm thick), the quartz crystal (8 × 8 mm and 250 µm thick), and the protective polymer cap with fluidic and electrical ports and a cavity housing the QCM without direct contact.

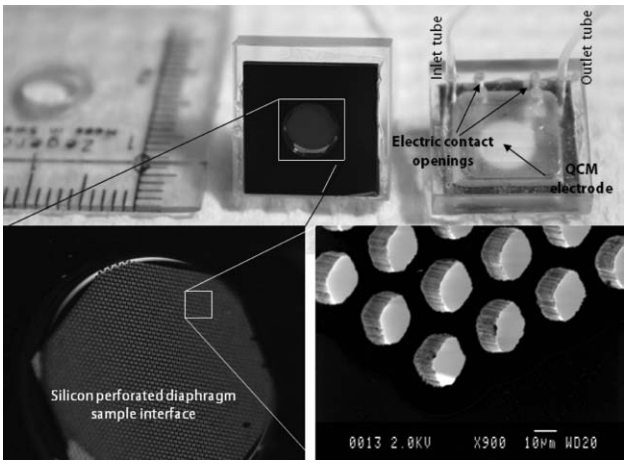

Fig. 7 Front and backside pictures of two devices. The QCM crystal is visible through the polymer backside cover. The SEM insert shows the 20 µm thick diaphragm with 18324 hexagon shaped 23 µm diameter perforations with wall thickness 10 µm.

Narcotics detection

Consecutive measurements with 200 ng and 300 ng ecstasy on the filter resulted in a respective baseline shift of 50 and 44 Hz, respectively, see Fig. 8a, whereas blank filter runs resulted in a signal level of at least an order of magnitude lower (<5 Hz, within noise limits). A third run with 200 ng ecstasy sample yielded 10 Hz. The decrease in signal is most likely caused by a depletion of antibodies on the QCM surface. However, this run shows that the surface is not completely depleted of antibodies, which could otherwise be the cause of the low signal level during the previous blank run. Similar system tests were also successfully performed with cocaine-prepared filters targeted at QCMs prepared with cocaine–Ag and cocaine–Ab chemistry, see Fig. 8b.

Discussion

The frequency shift response in tests with cocaine (~5 Hz per 100 ng) and with ecstasy (~15 Hz per 100 ng) corresponds to a sensitivity of at least 20 ng Hz^{-1} and 6 ng Hz^{-1}, respectively. However, the response probably corresponds to a lesser amount of drug since one can assume that sample losses occur during the transport of the drug from the filter sheet to the surface of the quartz crystal. The difference in sensitivity between the measurements of the two drug samples could be due to different amounts of heating of the filter sheets during sample loading or due to the different reaction kinetics of the two competitive binding assays. The sensitivity level is limited by noise, which was measured during blank runs to approximately 5 Hz, and by temperature and pressure fluctuations.

The interactions between the drugs, antibodies, and the immobilized antigens have not yet been fully characterized. Preliminary results from investigating the affinity of immobilized antibodies to the drug molecules were used in the simulations with the approximation that the affinity of the antibodies to the surface antigens is considerably lower. Furthermore, immobilization of antigens relies purely on physisorption. Neither the packing density nor the orientation of the molecules at the surface have been characterized and therefore the true number of available binding sites is uncertain. Without having the complete information of the kinetics of the competitive binding nor the number of binding sites, no numerical speculations are made on issues concerning the level of available antibodies after loading the system, the level of released antibody–drug complexes after introducing the sample, or on the efficiency in regeneration of the layer of antibodies on top of the immobilized antigens.

In this micromachined microfluidic device, capillary action and surface tension are dominating over gravity, thus the device is largely insensitive to moves, tilts, turning and repositioning. This results in a robust device that tolerates manual handling. The size and weight of the device and its low manufacturing cost can be compared to commercially available systems[21] that are large, heavy and expensive. Thus, the presented electronic drug sensing system fulfils foreseen demands of a handheld device for drug detection.

The assay chamber contains 0.98 µl and the perforations 0.21 µl. A 10 min run will use 3.5 µl of PBS and the chamber liquid volume will be refreshed 3 times. Thus, large liquid reservoirs are unnecessary which facilitates the use of the device in portable applications. In our experimental setup, we found the response time, *i.e.* the time between the start of the heat pulse and the time of a stable readout signal, to be approximately 25 s, where the heat pulse accounts for 5 or 8 s and the diffusion time for less than 5 s (estimated). In many security or health care applications a response time of 30 s is acceptable. The

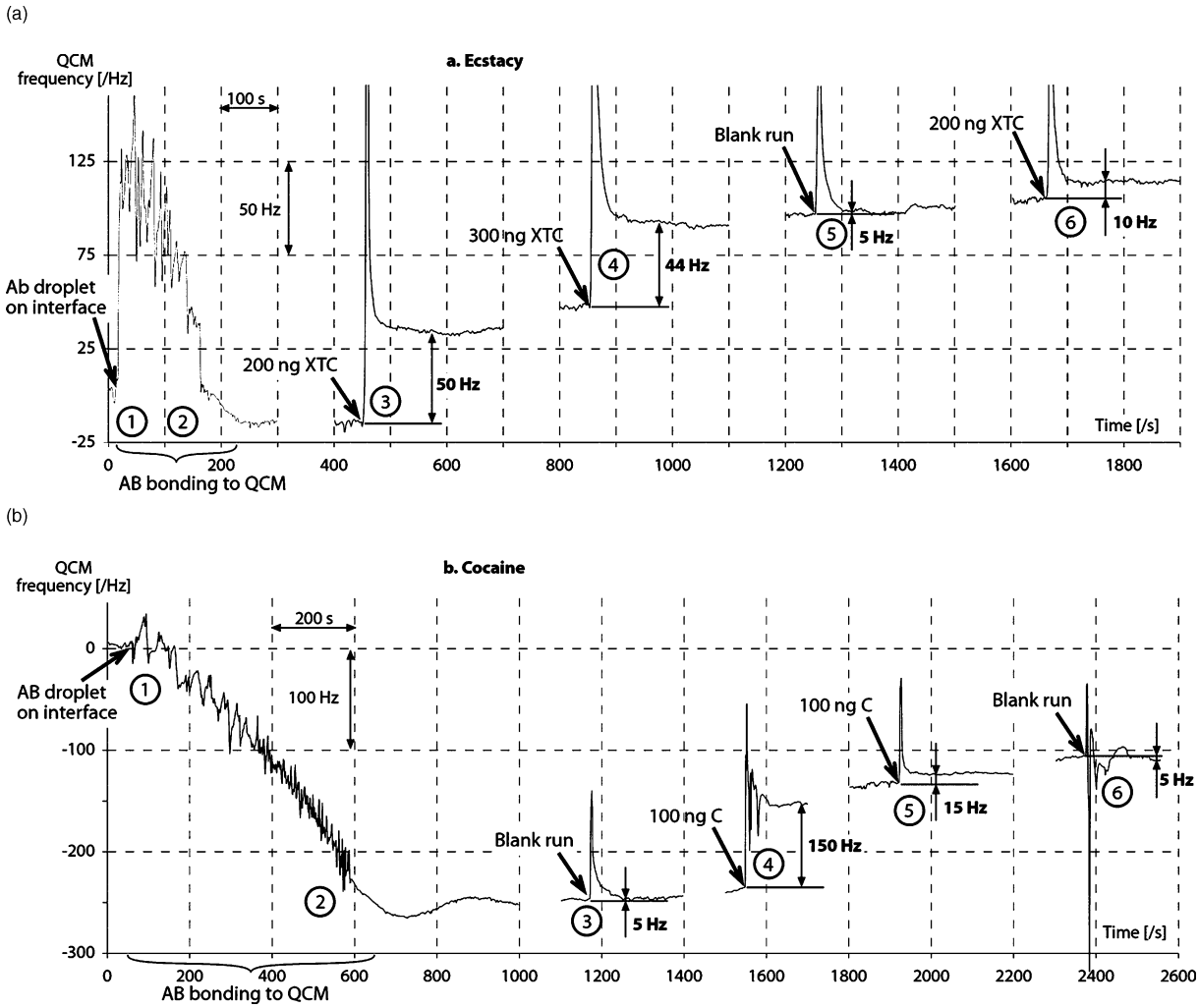

Fig. 8 (a) Measured system response to the subsequent loading of the system with (1) antibodies, (2) antibody binding, (3) 200 ng ecstasy loaded sample, (4) 300 ng ecstasy loaded sample and (5) a blank sample run. In order to verify that the system was not depleted from antibodies another run was made with 200 ng ecstasy loaded sample. Starting frequency 10 009 960 Hz. (b) Measured system response to the subsequent loading of the system with (1) antibodies targeted for cocaine, (2) antibody binding, (3) first blank run, (4) and (5) 100 ng cocaine loaded samples, (6) second blank sample run. Starting frequency 10 008 100 Hz.

finite element analysis simulations indicate that the depletion of antibodies at the QCM surface is achieved within 2 s, implying that there is room for further optimization and decrease of total measurement time. However, measurements show that the surface had not immediately been depleted in the real system since sequential tests still gave a read-out signal. This indicates that the heating of the fibreglass sheet only yielded a low amount of vaporized sample, there were substantial losses (such as parasitic binding) of sample during the transport from the sheet to the surface of the QCM, or the competitive immunoassay was non-optimized due to *e.g.* steric hindrance. As the detection chemistry relies on a liquid based immunoassay with drug molecules, antigens, and antibodies we believe that molecular diffusion is the dominant sample transport mechanism. The contribution from Marangoni and convective transport has not been studied. Integrating the sample interface and the QCM in very close proximity reduces the wet parasitic binding area as tubing and connectors between adsorption interface and assay sensor are unnecessary.

We found that the 3M 9703 VCAF performed sufficiently in terms of its main functional properties: sealing, electrical conductivity and the adhesion keeping the system parts together. Blister testing of the adhesive foil is a worst-case test, and with the adhesive foil confined between two rigid walls, *i.e.* the silicon frame and the quartz crystal, should yield even better results.[31] Our testing (see ESI)† of the VCAF with liquid pressures ranging from 1–60 kPa in combination with six common substrate materials shows the use of the adhesive for a range of microsystem applications.

Conclusions

With the use of a novel multifunctional adhesive material and a new geometric design, we achieved functional integration of a silicon sample interface between air and liquid and the QCM sensing element. Both fluidic connections as well as electrical contacting are incorporated in a single system with minimal assembly effort in a MEMS device. This results in low-cost

manufacturing and reduced system size and weight in comparison with commercially available systems. We successfully measured 100–200 ng of narcotics samples with a sensitivity ranging from 6–20 ng Hz^{-1}. The time required from sample loading to a signal read-out is kept below 30 s, which allows for fast analysis. The results are of relevance, both regarding the device size and the detection sensitivity and time for handheld instruments used to detect narcotics.

Acknowledgements

We would like to thank the Swedish Governmental Agency for Innovation Systems (VINNOVA) through the SUMMIT program for financial help.

References

1 M. Michalzik, R. Wilke and S. Büttgenbach, *Sens. Actuators, B*, 2005, 410–415.
2 C. Kösslinger, S. Drost, F. Aberl, H. Wolf, S. Koch and P. Woias, *Biosens. Bioelectron.*, 1992, **7**, 397–404.
3 T. Frisk, W. v. d. Wijngaart, D. Rönnholm and G. Stemme, *Lab Chip*, 2006, **6**, 1504–1509.
4 S. S. Sridharamurthy and H. Jiang, *IEEE Sens. J.*, 2007, **7**, 1315–1316.
5 A. Desai, S.-W. Lee and Y.-C. Tai, in *MEMS*, 2000, pp. 733–738.
6 Y. Zhao and S. K. Cho, *Lab Chip*, 2005, **6**, 137–144.
7 Y. Zhao, S. K. Chung, U.-C. Yi and S. K. Cho, in *MicroTAS*, Paris, 2007, pp. 847–849.
8 G. Sauerbrey, *Z. Phys.*, 1959, **155**, 206–222.
9 K. K. Kanazawa and J. G. Gordon, *Anal. Chim. Acta*, 1985, **175**, 99–105.
10 K. K. Kanazawa and J. G. Gordon, *Anal. Chem.*, 1985, **57**, 1770–1771.
11 A. P. M. Glassford, *J. Vac. Sci. Technol.*, 1978, **15**, 1836–1843.
12 C. Barnes, *Sens. Actuators, A*, 1991, **A**, 59–69.
13 B. A. Martin and H. E. Hager, *J. Appl. Phys.*, 1988, **66**, 2630–2636.
14 C.-C. L. S. Lin, H-F. Chien and S-M. Hsu, *J. Immunol. Methods*, 2000, **239**, 12–124.
15 B. A. Martin and H. E. Hager, *J. Appl. Phys.*, 1989, **66**, 2630–2636.
16 B. A. Martin and H. E. Hager, *J. Appl. Phys.*, 1989, **65**, 2627–2629.
17 P. Månsson, D. Rönnholm and Biosensor Applications AB, Biosensor Technology–An Introduction–Biosens(TM), A new era in vapor and trace detection, http://www.biosensor.se, Accessed 11 May 2005.
18 Q-sense, Tracking changes at the surface, http://www.q-sense.com, Accessed April 2008.
19 Attana, Understanding molecules, http://www.attana.com, Accessed April 2008.
20 Biosensor, Collect Trace Analyze, http://www.biosensor.se, Accessed April 2008.
21 P. Månsson, H. Andersson, J. Smith, K. Jensen and T. Aastrup, *Pat.*, PCT/SE2003/001038, 2003.
22 P. Månsson, J. Smith and A.-C. Hellgren, *Pat.*, PCT/SE2002/002098, 2003.
23 W. C. Young and R. G. Budynas, *Roark's Formulas for Stress and Strain*, McGraw-Hill, New York, 2002.
24 K. E. Petersen, *Proc. IEEE*, 1982, **70**, 420–457.
25 J. Melin, W. v. d. Wijngaart and G. Stemme, *Lab Chip*, 2005, **5**.
26 D. D. Meng, J. Kim and C.-J. Kim, *J. Micromech. Microeng.*, 2006, **16**, 419–424.
27 J. Melin, N. Roxhed, G. Gimenez, P. Griss, W. v. d. Wijngaart and G. Stemme, *Sens. Actuators, B*, 2004, **100**, 463–468.
28 K. Handique, B. P. Gogoi, D. T. Burke, C. H. Mastrangelo and M. A. Burns, *Proc. SPIE–Int. Soc. Opt. Eng.*, 1997, **3224**, 185–195.
29 J. Pellicer, V. Garcia-Morales and M. Hernandez, *Phys. Educ.*, 2000, **35**, 126–130.
30 T. Gervais and K. F. Jensen, *Chem. Eng. Sci.*, 2006, **61**(2006), 1102–1121.
31 U. Kulmi and S. Basu, *Model. Simul. Mater. Sci. Eng.*, 2006, 1071–1093.